Applied Physics Letters

Lossless plasmons in highly mismatched alloys

Cite as: Appl. Phys. Lett. **120**, 252102 (2022); https://doi.org/10.1063/5.0095766
Submitted: 12 April 2022 • Accepted: 09 June 2022 • Published Online: 21 June 2022

Hassan Allami and Jacob J. Krich

View Online Export Citation CrossMark

ARTICLES YOU MAY BE INTERESTED IN

Surface plasmon-assisted control of the phase of photo-induced spin precession
Applied Physics Letters **120**, 251101 (2022); https://doi.org/10.1063/5.0097539

High-frequency conductivity and temperature dependence of electron effective mass in AlGaN/GaN heterostructures
Applied Physics Letters **120**, 252103 (2022); https://doi.org/10.1063/5.0093292

Ternary organic solar cells: Insights into charge and energy transfer processes
Applied Physics Letters **120**, 250501 (2022); https://doi.org/10.1063/5.0096556

Webinar
Meet the Lock-in Amplifiers that measure microwaves
Oct. 6th – Register now
Zurich Instruments

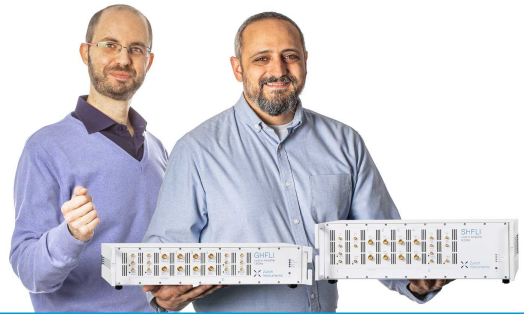

© 2022 Author(s).

Applied Physics Letters ARTICLE scitation.org/journal/apl

Lossless plasmons in highly mismatched alloys

Cite as: Appl. Phys. Lett. **120**, 252102 (2022); doi: 10.1063/5.0095766
Submitted: 12 April 2022 · Accepted: 9 June 2022 ·
Published Online: 21 June 2022

View Online Export Citation CrossMark

Hassan Allami[a] and Jacob J. Krich[b]

AFFILIATIONS

Department of Physics, University of Ottawa, Ottawa, Ontario K1N 6N5, Canada

[a]Author to whom correspondence should be addressed: hassan.allami@gmail.com
[b]School of Electrical Engineering and Computer Science, University of Ottawa, Ottawa, Ontario ON K1N 6N5, Canada.

ABSTRACT

We explore the potential of highly mismatched alloys (HMAs) for realizing lossless plasmonics. Systems with a plasmon frequency at which there are no interband or intraband processes possible are called lossless, as there is no two-particle loss channel for the plasmon. We find that the band splitting in HMAs with a conduction band anticrossing guarantees a lossless frequency window. When such a material is doped, producing plasmonic behavior, we study the conditions required for the plasmon frequency to fall in the lossless window, realizing lossless plasmons. Considering a generic class of HMAs with a conduction band anticrossing, we find universal contours in their parameter space within which lossless plasmons are possible for some doping range. Our analysis shows that HMAs with heavy effective masses and small high-frequency permittivity are most promising for realizing a lossless plasmonic material.

Published under an exclusive license by AIP Publishing. https://doi.org/10.1063/5.0095766

The field of plasmonics relies on surface plasmon polariton (SPP) modes, which can be excited on metal–dielectric interfaces.[1,2] These SPP modes can enhance and concentrate electric fields at subwavelength scale,[3–5] with applications in metamaterials,[6] optoelectronics,[7–12] and photocatalysis.[13] The applications range from the established surface-enhanced Raman scattering (SERS) technique[14] to new proposals in quantum optics[15] such as quantum teleportation.[16]

In practice, many plasmonic applications are hindered by loss and decay of the plasmonic modes.[17–19] Although some plasmonic applications such as SERS are still viable in the presence of losses,[20] and in cases such as photodetection and photocatalysis losses are beneficial,[12,13,17,21] the loss problem is one of the main challenges in the fields of plasmonics and metamaterials.[6,22]

Many approaches have been proposed to reduce and mitigate losses in plasmonic systems, including improvements in fabrication,[23] employing optical gain,[24] spectrum modification,[25] and, of course, searching for alternative plasmonic materials.[26–31] Khurgin and Sun presented a strategy to find lossless plasmonic modes by considering the fundamental conditions creating loss.[32] Often, the most important loss channel for SPPs is decay into electron–hole excitation. They argue that dissipating the energy of an electromagnetic mode in this way requires empty electronic states. In a material with the appropriate electronic structure, such empty states may be absent for a range of energies, offering a lossless window of frequencies. Hence, they conclude that if the plasma frequency falls inside the lossless window, the primary decay mechanism will have been removed, producing an essentially lossless plasmonic material. Khurgin and Sun proposed a few classes of materials that can potentially realize their conditions for lossless plasmons, and some of them have been investigated with promising results.[33–35]

In this work, we propose highly mismatched alloys (HMA) as a candidate class for realizing mid- to far-IR lossless plasmons. This possibility was briefly mentioned but not elaborated in Ref. 36. We consider the one-particle and plasmonic structure of HMAs and find the alloying and doping requirements to achieve lossless plasmons. We describe universal contours in the parameter space of HMAs in which lossless plasmons are possible for some range of doping. These contours show that HMAs with large effective masses and small high-frequency permittivity ε_∞ are most likely to be able to realize the conditions needed for lossless plasmons with reasonable frequency. We consider the most-studied HMAs with conduction-band anticrossings, ZnCdTeO and GaPAsN, and show that they are unable to realize lossless plasmons when the alloy fraction x is larger than 10^{-8}, due to the light effective masses of the host bands and ε_∞. We conclude by describing the properties of desirable materials and discussing one candidate: MgO. In the remainder of this work, we use the term "lossless window" in the sense of Ref. 32.

HMAs are a class of semiconductor alloys where the alloying elements have very different electronegativity than that of the host. Reference 37 described that localized states form around the mismatching elements and proposed a band anticrossing (BAC) model, which successfully describes the energy spectrum of HMAs. According to the

Published under an exclusive license by AIP Publishing

BAC model, the localized level E_d and the host conduction band (CB) with dispersion $E_{\mathbf{k}}$ hybridize at each wavevector $\mathbf{k}$ independently with a single coupling factor V, while the valence bands (VBs) are not affected,[38] as depicted in Fig. 1. The CB splits into two new bands, with dispersion

$$E_{\pm} = \frac{1}{2}\left(E_k + E_d \pm \sqrt{(E_k - E_d)^2 + 4V^2 x}\right), \tag{1}$$

where x is the alloy fraction of the mismatching element. The two split bands $E_{\pm}$ are shown as solid black curves in Fig. 1. When E_d is far from the VB edge, both the emergence of the $E_{\pm}$ bands and that the VB is largely unchanged are supported by various first principles calculations of band structure[39–41] and optical properties[42–44] for a range of HMAs, tight-binding and $\mathbf{k}\cdot\mathbf{p}$ models,[45,46] and experimental studies.[47,48] Here, we consider a class of HMAs where the localized level anticrosses with a parabolic CB with $E_{\mathbf{k}} = \hbar^2 k^2/2m$, the bottom of which is taken to be the zero energy level, as shown in Fig. 1. All such HMAs are described by three scalar parameters: $V\sqrt{x}$, E_d, and m.

We now describe the range of excitation energies that can be lost to particle–hole excitations in a doped HMA. We consider that the excess electrons occupy the E_- band, and we consider the temperature to be small compared to the energy gaps in the problem, so the chemical potential μ lies somewhere in E_-, as in Fig. 1. Although E_- is a narrow band, it inherits a part of the propagating states of the original CB, and it is not perfectly flat. Exotic physics such as the Mott transition or other correlation-induced states has not been observed in doped HMAs. Rather, we expect that the free electrons in E_- produce plasmonic behavior[49] while, at the same time, providing two channels for dissipating energy. First, an excitation of any amount of energy up to the bandwidth ΔE_- of the E_- band can move an electron from a filled state to an empty state within the E_- band. The excited electron and hole can then dissipate their energy into a set of excitations with infinitesimal energy by moving electrons near the Fermi surface to nearby empty states. Figure 2 shows the range of excitation energies and μ where dissipation into particle–hole excitations can occur; the gray area under the horizontal dashed red line represents this intraband

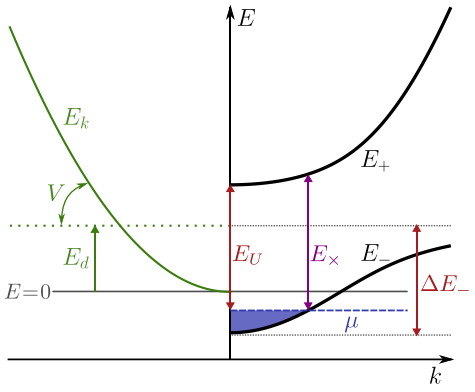

FIG. 1. (left) The conduction band of the host material E_k and the localized state E_d, coupled through V. The energy reference is at the bottom of E_k. (right) The split bands of the BAC model, E_+ and E_-. The interband loss starts for energies larger than E_U, and for the energies below E_- bandwidth ΔE_-, intraband dissipation is possible. Doping determines the chemical potential μ. The interband transitions bound plasmon energy $\hbar\omega_p$ to $E_\times = \min_{k<k_F}(E^+_{\mathbf{k}} - E^-_{\mathbf{k}})$.

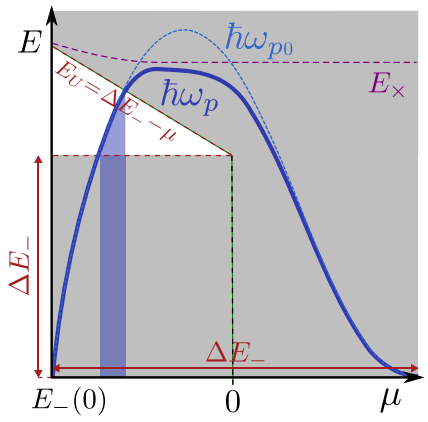

FIG. 2. The lossless window of excitation energies (white area) and $\hbar\omega_p$ (dark blue line) as a function of chemical potential μ. $\hbar\omega_p$ is bounded by $\hbar\omega_{p0}$ and $E_\times$. The blue shaded strip shows the range of μ where $\hbar\omega_p$ falls in the lossless window.

lossy region. Second, an electron can be excited to the E_+ band. The minimum energy for such interband transitions is $E_U \equiv E_+(k=0) - \mu$, which is labeled in Figs. 1 and 2. Excitations with energy higher than E_U can then be lost through a combination of inter- and intraband transitions. The gray area above the slanted dashed line in Fig. 2 represents the second lossy region. In principle, it is possible that an excitation with energy larger than ΔE_- generates two electron–hole pairs through electron–electron scattering within E_-. However, such processes, which are beyond the Khurgin and Sun scheme, require Umklapp scattering,[50] which is not likely in the lossless HMAs. The lossless plasmons in these HMAs are achievable in low-doping regimes, where the Fermi momentum k_F is small. So for Umklapp processes, the two electrons involved need to scatter to large momenta. However, E_- is mainly made out of the localized states at large momenta and has a vanishing weight.[49] The phase space for creating two electron–hole pairs with the electrons at large momenta with total energy larger than ΔE_- and smaller than E_U is negligibly small.

Excitations with energy between ΔE_- and E_U are lossless, i.e., have no single-particle decay channels, if $E_U > \Delta E_-$. The white area in Fig. 2 shows this lossless window, which linearly shrinks with increasing μ. Measuring energies from the bottom of $E_{\mathbf{k}}$, it turns out that $E_+(k=0) = \Delta E_-$, so $E_U = \Delta E_- - \mu$. So, there is always a lossless window if $\mu < 0$. Moreover, since the minimum of E_- is always negative, for any HMA, there is always a doping level below which there exists a lossless window.

The next step is to check when the plasmon energy $\hbar\omega_p$ falls in the lossless window. $\hbar\omega_p$ depends on the carrier concentration and hence on μ, which ranges between the bottom and the top of E_- at zero temperature. As shown by the blue curve in Fig. 2, $\hbar\omega_p$ initially rises with μ as free carriers enter the E_- band and fall back to zero when the band is full.[49] Depending on the HMA parameters, $\hbar\omega_p$ can fall in the lossless window for some range of doping, as in the case in the figure.

In previous work,[49] using a single-particle Green's function that describes the disorder-averaged propagation in a system consisting of the original CB and the defect level, we determined ω_p. Here, we also include ε_∞ to phenomenologically account for the screening effect of

Published under an exclusive license by AIP Publishing

processes much faster than ω_p, including interband transitions to remote bands. The result is

$$\omega_p^2 = \omega_{p0}^2\left[1 + \left(\frac{mc\ell}{\hbar\varepsilon_\infty}\right)^2 I_\times(\omega_p)\right]^{-1}, \quad (2)$$

in which ω_{p0} is the reduced plasma frequency in the absence of $E_- \to E_+$ transitions, and the second term in the bracket represents the effect of such transitions, where ℓ is a length scale that determines their strength, which needs to be determined for each HMA. We provide more details in Section A of the supplementary material. Reference 49 derived a closed algebraic form for ω_{p0} and an integral for $I_\times(\omega)$, which has a singularity at $\hbar\omega = E_\times \equiv \min_{k<k_F}(E^+_{\mathbf{k}} - E^-_{\mathbf{k}})$, where k_F is the Fermi momentum. Interband transitions are only important when $\hbar\omega_{p0}$ is close to or larger than $E_\times$ and typically keep $\hbar\omega_p$ below $E_\times$, as Fig. 2 shows. Note that since $E_\times$ is the minimum distance between E_+ and the filled part of E_- at the same $\mathbf{k}$, it is always larger than E_U, which does not have the same $\mathbf{k}$ restriction (see Figs. 1 and 2).

If we normalize all energies to $E_m \equiv 2mc^2/\varepsilon_\infty^2 \times 10^{-9}$, then we can accommodate this entire class of HMAs in a 2D plane spanned by $\tilde{V}\sqrt{x} \equiv V\sqrt{x}/E_m$ and $\tilde{E}_d \equiv E_d/E_m$. Since $2mc^2$ is of the order of MeV for typical semiconductors, the factor of 10^{-9} brings E_m to the more relevant meV range. For the bare electron mass m_e and $\varepsilon_\infty = 1$, $E_m \approx 1$ meV, so for any other effective mass m and ε_∞, one can scale all dimensionless energies by $m/m_e\varepsilon_\infty^2$ to find the approximate value in meV. Section A of the supplementary material shows why the normalization factor ε_∞^2 appears.

We can determine for any point in the $(\tilde{V}\sqrt{x}, \tilde{E}_d)$ plane whether there is a doping range in which $\hbar\omega_p$ falls in the lossless window, realizing lossless plasmons. Then, with fixed $\tilde{\ell} \equiv \ell mc/\hbar\varepsilon_\infty$, where $\hbar/mc$ is the reduced Compton wavelength, there is a universal contour in the $(\tilde{V}\sqrt{x}, \tilde{E}_d)$ plane within which such HMAs fall. Figure 3 shows these universal contours of lossless plasmonic HMAs for a few values of $\tilde{\ell}$. The solid black contour shows the $\ell = 0$ case without interband transitions, where $\omega_p = \omega_{p0}$. The contours do not vary significantly from the $\tilde{\ell} = 0$ case until $\tilde{\ell} \gtrsim 100$ since $I_\times(\omega)$ in Eq. (2) is significant only for $\hbar\omega_p$ near $E_\times$. However, since in the lossless window $\hbar\omega_p < E_U < E_\times$, the interband processes can move $\hbar\omega_p$ away from $\hbar\omega_{p0}$ only when $\tilde{\ell}$ is large. For estimated typical values of $\ell = 1 - 10$ Å, $\tilde{\ell} \approx (250\text{–}2500)\mathrm{m/m_e}\varepsilon_\infty$. Using ω_{p0} in place of ω_p, as in the $\tilde{\ell} = 0$ case, allows us to derive an analytic expression for the lossless contour, which is presented in Section B of the supplementary material.

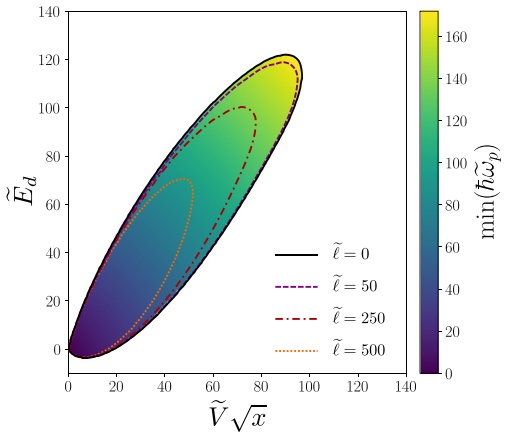

FIG. 3. Universal contours showing regions with lossless plasmons for several $\tilde{\ell} \equiv mc\ell/\hbar\varepsilon_\infty$, with energies all normalized by $E_m \equiv 2mc^2/\varepsilon_\infty^2 \times 10^{-9}$. The color scale shows the smallest normalized plasmon energy in the lossless window, which is always equal to $\Delta E_-/E_m$, independent of $\tilde{\ell}$.

The color scale of Fig. 3 shows the smallest $\hbar\tilde{\omega}_p$ in the lossless window. As Fig. 2 shows, the minimum value of $\hbar\omega_p$ in the lossless window is always ΔE_-, which does not depend on ℓ. Therefore, $\min(\hbar\omega_p/E_m)$ is the same for lossless contours belonging to different $\tilde{\ell}$. Although the largest $\hbar\tilde{\omega}_p$ in the lossless window is somewhat different for each $\tilde{\ell}$, the typical difference between $\max(\hbar\omega_p)$ and $\min(\hbar\omega_p)$ is of the order of a few E_m for all cases.

Since $E_m \propto m/\varepsilon_\infty^2$, Fig. 3 shows that HMAs with heavier m and smaller ε_∞ can achieve lossless plasmons for a wider range of $V\sqrt{x}$ and E_d. Since the typical values of V are of the order of eV, increasing the range of $V\sqrt{x}$ is particularly crucial because otherwise the required x may be too small to realistically show alloying effects.

To illustrate this point, consider two standard quaternary HMAs, $Zn_{1-y}Cd_yTe_{1-x}O_x$ in which oxygen is the mismatching element, and the classic HMA, $GaP_zAs_{1-z-x}N_x$, where nitrogen is the mismatching element. Table I shows the range of BAC parameters for these quaternaries, determined from studies of alloy-dependent bandgap[45,51–54] as well as ε_∞ value for the corresponding hosts.[55] Doping of the E_- band of these HMAs has, for example, been demonstrated with chlorine in ZnCdTeO.[56] In both quaternaries, E_d is tunable and goes from negative to positive by changing y or z, as Table I shows. Given the small $m/m_e\varepsilon_\infty^2$ for these standard HMAs, E_d needs to be near zero for them to be inside the lossless contour. Using bowing parameters $C_1 = 0.46$ eV for ZnCdTe[51] and $C_2 = 0.19$ eV for GaPAs,[53] obtaining $E_d \approx 0$ requires $y \approx 0.318$ and $z \approx 0.274$. Then, using linear interpolation of the values listed in Table I for V, m, and ε_∞, we find $m/m_e\varepsilon_\infty^2 \approx 2.26 \times 10^{-3}$ for ZnCdTe and $m/m_e\varepsilon_\infty^2 \approx 8.3 \times 10^{-4}$ for GaPAs. The result is that the maximum value of x for which $Zn_{1-y}Cd_yTe_{1-x}O_x$ falls in the lossless contour is 5.8×10^{-9}, and it is 7.8×10^{-10} for $GaP_zAs_{1-z-x}N_x$. With such small x values, the gap between the E_- and E_+ bands is not truly developed, so the lossless plasmon in E_- band is more a formal statement than a realizable result. Moreover, with the small $m/m_e\varepsilon_\infty^2$ in these cases, the available $\hbar\omega_p$ in the lossless contour is always less than 1 meV. For such small $\hbar\omega_p$, phonons could directly couple to the plasmons, providing a new channel for dissipation and breaking the lossless condition.

TABLE I. The range of BAC parameters and ε_∞ for $Zn_{1-y}Cd_yTe_{1-x}O_x$ and $GaP_zAs_{1-z-x}N_x$.[45,51–55]

Parameters	$y=0$	$y=1$	$z=0$	$z=1$
E_d (eV)	−0.27	0.38	0.22	−0.6
V (eV)	2.8	2.2	2.8	3.05
m (m_e)	0.117	0.09	0.067	0.13
ε_∞	6.9	7.1	10.86	8.8

Published under an exclusive license by AIP Publishing

The existing HMAs with CB anticrossing may not be able to realize lossless plasmons, but they should still show the suppression of electronic decay channels in the lossless window in experiments. Our lossless contour map shows that a material with a heavier effective mass and smaller ε_∞ would allow both for larger x and lossless plasmons with higher $\hbar\omega_p$. Even for possible yet-to-be-characterized HMAs with larger $m/m_e\varepsilon_\infty^2$, the lossless plasmons likely will be in the THz to far-IR range. Observing these low plasma frequencies may require low temperatures, as Eq. (2) is derived in the low temperature limit. At higher temperatures, the occupation fraction of states in the E_- band must be taken into account.

Although overall HMAs with heavier m and smaller ε_∞ are more promising in realizing lossless plasmons, not everything favors them. Interband transitions shrink the lossless contour, as shown in Fig. 3, and $\tilde{\ell}$ increases linearly with m/ε_∞.

HMAs with valence band anticrossings[57,58] could be good candidates, as they typically have heavier effective masses, though the theory of their plasmon frequencies has not yet been worked out. For instance, MgO has heavy holes with $m \approx 2m_e$ and $\varepsilon_\infty \approx 3$,[59] so could be a candidate host for an HMA capable of realizing lossless hole plasmons. Despite serious challenges, HMAs present exciting potential for realizing a lossless plasmonic medium and are worth more theoretical and experimental investigations.

See the supplementary material for the details of the plasma frequency equation and the analytic expression of the lossless contour for the case of $\ell = 0$.

We acknowledge funding from the NSERC CREATE TOPSET program under Award No. 497981.

AUTHOR DECLARATIONS

Conflict of Interest

The authors have no conflicts to disclose.

Author Contributions

Hassan Allami: Conceptualization (equal); Data curation (equal); Formal analysis (equal); Investigation (equal); Methodology (equal); Validation (equal); Visualization (equal); Writing – original draft (equal); Writing – review and editing (equal). **Jacob J. Krich:** Conceptualization (equal); Funding acquisition (lead); Investigation (supporting); Methodology (supporting); Project administration (lead); Resources (lead); Supervision (lead); Validation (equal); Visualization (supporting); Writing – original draft (equal); Writing – review and editing (equal).

DATA AVAILABILITY

The data that support the findings of this study are openly available in Lossless HMAs at https://github.com/hassan-allami/Lossless-HMAs, Ref. 60.

REFERENCES

[1]R. H. Ritchie, "Plasma losses by fast electrons in thin films," Phys. Rev. **106**, 874–881 (1957).
[2]C. J. Powell and J. B. Swan, "Effect of oxidation on the characteristic loss spectra of aluminum and magnesium," Phys. Rev. **118**, 640–643 (1960).
[3]S. A. Maier, *Plasmonics: Fundamentals and Applications* (Springer, 2007).
[4]W. L. Barnes, A. Dereux, and T. W. Ebbesen, "Surface plasmon subwavelength optics," Nature **424**, 824–830 (2003).
[5]E. Ozbay, "Plasmonics: Merging photonics and electronics at nanoscale dimensions," Science **311**, 189–193 (2006).
[6]A. M. Urbas, Z. Jacob, L. D. Negro, N. Engheta, A. D. Boardman, P. Egan, A. B. Khanikaev, V. Menon, M. Ferrera, N. Kinsey, C. DeVault, J. Kim, V. Shalaev, A. Boltasseva, J. Valentine, C. Pfeiffer, A. Grbic, E. Narimanov, L. Zhu, S. Fan, A. Alù, E. Poutrina, N. M. Litchinitser, M. A. Noginov, K. F. MacDonald, E. Plum, X. Liu, P. F. Nealey, C. R. Kagan, C. B. Murray, D. A. Pawlak, I. I. Smolyaninov, V. N. Smolyaninova, and D. Chanda, "Roadmap on optical metamaterials," J. Opt. **18**, 093005 (2016).
[7]M. Kauranen and A. V. Zayats, "Nonlinear plasmonics," Nat. Photonics **6**, 737–748 (2012).
[8]X. Guo, Y. Ma, Y. Wang, and L. Tong, "Nanowire plasmonic waveguides, circuits and devices," Laser Photonics Rev. **7**, 855–881 (2013).
[9]Z. Han and S. I. Bozhevolnyi, "Radiation guiding with surface plasmon polaritons," Rep. Prog. Phys. **76**, 016402 (2013).
[10]M. I. Stockman, "The spaser as a nanoscale quantum generator and ultrafast amplifier," J. Opt. **12**, 024004 (2010).
[11]H. A. Atwater and A. Polman, "Plasmonics for improved photovoltaic devices," in *Materials for Sustainable Energy* (World Scientific, 2011), pp. 1–11.
[12]M. Li, S. K. Cushing, and N. Wu, "Plasmon-enhanced optical sensors: A review," Analyst **140**, 386–406 (2015).
[13]W. Hou and S. B. Cronin, "A review of surface plasmon resonance-enhanced photocatalysis," Adv. Funct. Mater. **23**, 1612–1619 (2013).
[14]M. Fleischmann, P. Hendra, and A. McQuillan, "Raman spectra of pyridine adsorbed at a silver electrode," Chem. Phys. Lett. **26**, 163–166 (1974).
[15]M. S. Tame, K. McEnery, Ş. Özdemir, J. Lee, S. A. Maier, and M. Kim, "Quantum plasmonics," Nat. Phys. **9**, 329–340 (2013).
[16]X. Jiang, P. Chen, K. Qian, Z. Chen, S. Xu, Y. Xie, S. Zhu, and X. Ma, "Quantum teleportation mediated by surface plasmon polariton," Sci. Rep. **10**, 11503 (2020).
[17]S. V. Boriskina, T. A. Cooper, L. Zeng, G. Ni, J. K. Tong, Y. Tsurimaki, Y. Huang, L. Meroueh, G. Mahan, and G. Chen, "Losses in plasmonics: From mitigating energy dissipation to embracing loss-enabled functionalities," Adv. Opt. Photonics **9**, 775–827 (2017).
[18]J. B. Khurgin and A. Boltasseva, "Reflecting upon the losses in plasmonics and metamaterials," MRS Bull. **37**, 768–779 (2012).
[19]J. B. Khurgin and G. Sun, "Scaling of losses with size and wavelength in nanoplasmonics and metamaterials," Appl. Phys. Lett. **99**, 211106 (2011).
[20]J. B. Khurgin, "How to deal with the loss in plasmonics and metamaterials," Nat. Nanotechnol. **10**, 2–6 (2015).
[21]G. Baffou and R. Quidant, "Thermo-plasmonics: Using metallic nanostructures as nano-sources of heat," Laser Photonics Rev. **7**, 171–187 (2013).
[22]M. I. Stockman, K. Kneipp, S. I. Bozhevolnyi, S. Saha, A. Dutta, J. Ndukaife, N. Kinsey, H. Reddy, U. Guler, V. M. Shalaev, A. Boltasseva, B. Gholipour, H. N. S. Krishnamoorthy, K. F. MacDonald, C. Soci, N. I. Zheludev, V. Savinov, R. Singh, P. Groß, C. Lienau, M. Vadai, M. L. Solomon, I. Barton, D. R. M. Lawrence, J. A. Dionne, S. V. Boriskina, R. Esteban, J. Aizpurua, X. Zhang, S. Yang, D. Wang, W. Wang, T. W. Odom, N. Accanto, P. M. de Roque, I. M. Hancu, L. Piatkowski, N. F. van Hulst, and M. F. Kling, "Roadmap on plasmonics," J. Opt. **20**, 043001 (2018).
[23]Y. Wu, C. Zhang, N. M. Estakhri, Y. Zhao, J. Kim, M. Zhang, X. Liu, G. K. Pribil, A. Alù, C. Shih, and X. Li, "Intrinsic optical properties and enhanced plasmonic response of epitaxial silver," Adv. Mater. **26**, 6106–6110 (2014).
[24]M. I. Stockman, "Nanoplasmonics: Past, present, and glimpse into future," Opt. Express **19**, 22029–22106 (2011).
[25]B. Luk'yanchuk, N. I. Zheludev, S. A. Maier, N. J. Halas, P. Nordlander, H. Giessen, and C. T. Chong, "The fano resonance in plasmonic nanostructures and metamaterials," Nat. Mater. **9**, 707–715 (2010).
[26]G. V. Naik, V. M. Shalaev, and A. Boltasseva, "Alternative plasmonic materials: Beyond gold and silver," Adv. Mater. **25**, 3264–3294 (2013).
[27]P. West, S. Ishii, G. Naik, N. Emani, V. Shalaev, and A. Boltasseva, "Searching for better plasmonic materials," Laser Photonics Rev. **4**, 795–808 (2010).
[28]G. V. Naik, J. Liu, A. V. Kildishev, V. M. Shalaev, and A. Boltasseva, "Demonstration of Al:ZnO as a plasmonic component for near-infrared metamaterials," Proc. Natl. Acad. Sci. U. S. A. **109**, 8834–8838 (2012).

Published under an exclusive license by AIP Publishing

[29]G. V. Naik, J. L. Schroeder, X. Ni, A. V. Kildishev, T. D. Sands, and A. Boltasseva, "Titanium nitride as a plasmonic material for visible and near-infrared wavelengths," Opt. Mater. Express **2**, 478–489 (2012).
[30]S. Law, D. C. Adams, A. M. Taylor, and D. Wasserman, "Mid-infrared designer metals," Opt. Express **20**, 12155–12165 (2012).
[31]P. Jung, A. V. Ustinov, and S. M. Anlage, "Progress in superconducting metamaterials," Supercond. Sci. Technol. **27**, 073001 (2014).
[32]J. B. Khurgin and G. Sun, "In search of the elusive lossless metal," Appl. Phys. Lett. **96**, 181102 (2010).
[33]H. Kim, "Novel plasmon resonances of nonstoichiometric alumina," Appl. Surf. Sci. **488**, 648–655 (2019).
[34]M. N. Gjerding, M. Pandey, and K. S. Thygesen, "Band structure engineered layered metals for low-loss plasmonics," Nat. Commun. **8**, 15133 (2017).
[35]J. B. Khurgin, "Mitigating the loss in plasmonics and metamaterials," Technical Report No. OMB NO. 0704-0188 (Johns Hopkins University, Baltimore, 2017).
[36]B. Saha, A. Shakouri, and T. D. Sands, "Rocksalt nitride metal/semiconductor superlattices: A new class of artificially structured materials," Appl. Phys. Rev. **5**, 021101 (2018).
[37]W. Shan, W. Walukiewicz, J. W. Ager, E. E. Haller, J. F. Geisz, D. J. Friedman, J. M. Olson, and S. R. Kurtz, "Band anticrossing in GaInNAs alloys," Phys. Rev. Lett. **82**, 1221–1224 (1999).
[38]W. Walukiewicz, K. Alberi, J. Wu, W. Shan, K. M. Yu, and J. W. Ager, "Electronic band structure of highly mismatched semiconductor alloys," in *Dilute III-V Nitride Semiconductors and Material Systems: Physics and Technology*, edited by A. Erol (Springer Berlin Heidelberg, Berlin, Heidelberg, 2008), Chap. III, pp. 65–89.
[39]M. P. Polak, R. Kudrawiec, and O. Rubel, "Electronic band structure of nitrogen diluted Ga(PAsN): Formation of the intermediate band, direct and indirect optical transitions, and localization of states," J. Appl. Phys. **126**, 175701 (2019).
[40]K. Sakamoto and H. Yaguchi, "First-principles study on the conduction band electron states of GaAsN alloys," Phys. Status Solidi C **11**, 911–913 (2014).
[41]C. Tablero, A. Martí, and A. Luque, "Analyses of the intermediate energy levels in ZnTe:O alloys," Appl. Phys. Lett. **96**, 121104 (2010).
[42]A. Gueddim, S. Zerroug, and N. Bouarissa, "Optical characteristics of $ZnTe_{1-x}O_x$ alloys from first-principles calculations," J. Lumin. **135**, 243–247 (2013).
[43]B. Lee and L. Wang, "Electronic structure of ZnTe:O and its usability for intermediate band solar cell," Appl. Phys. Lett. **96**, 071903 (2010).
[44]Y. Gohda and S. Tsuneyuki, "Optical conductivity of highly mismatched GaP alloys," Appl. Phys. Lett. **102**, 023901 (2013).
[45]R. Kudrawiec, A. V. Luce, M. Gladysiewicz, M. Ting, Y. J. Kuang, C. W. Tu, O. D. Dubon, K. M. Yu, and W. Walukiewicz, "Electronic band structure of $GaN_xP_yAs_{1-x-y}$ highly mismatched alloys: Suitability for intermediate-band solar cells," Phys. Rev. Appl. **1**, 034007 (2014).
[46]E. P. O'Reilly, A. Lindsay, S. Tomić, and M. Kamal-Saadi, "Tight-binding and k-p models for the electronic structure of Ga(In)NAs and related alloys," Semicond. Sci. Technol. **17**, 870–879 (2002).
[47]M. Welna, Ł. Janicki, W. M. Linhart, T. Tanaka, K. M. Yu, R. Kudrawiec, and W. Walukiewicz, "Effects of the host conduction band energy on the electronic band structure of ZnCdTeO dilute oxide alloys," J. Appl. Phys. **126**, 083106 (2019).
[48]K. Zelazna, M. Gladysiewicz, M. Polak, S. Almosni, A. Létoublon, C. Cornet, O. Durand, W. Walukiewicz, and R. Kudrawiec, "Nitrogen-related intermediate band in P-rich $GaN_xP_yAs_{1-x-y}$ alloys," Sci. Rep. **7**, 15703 (2017).
[49]H. Allami and J. J. Krich, "Plasma frequency in doped highly mismatched alloys," Phys. Rev. B **103**, 035201 (2021).
[50]J. B. Khurgin, "Hot carriers generated by plasmons: Where are they generated and where do they go from there?," Faraday Discuss. **214**, 35–58 (2019).
[51]T. Tanaka, K. Mizoguchi, T. Terasawa, Y. Okano, K. Saito, Q. Guo, M. Nishio, K. M. Yu, and W. Walukiewicz, "Compositional dependence of optical transition energies in highly mismatched $Zn_{1-x}Cd_xTe_{1-y}O_y$ alloys," Appl. Phys. Express **9**, 021202 (2016).
[52]S. Adachi, *Properties of Group-IV, III-V and II-VI Semiconductors* (John Wiley & Sons, 2005), Chap. VII, p. 150.
[53]I. Vurgaftman, J. R. Meyer, and L. R. Ram-Mohan, "Band parameters for III–V compound semiconductors and their alloys," J. Appl. Phys. **89**, 5815–5875 (2001).
[54]S. Adachi, "Energy-band structure: Energy-band gaps," in *Properties of Semiconductor Alloys* (John Wiley & Sons, Ltd, 2009), Chap. VI, pp. 133–228.
[55]S. Adachi, *Properties of group-IV, III-V and II-VI Semiconductors* (John Wiley & Sons, 2005), Chap. X, p. 218.
[56]T. Tanaka, K. Matsuo, K. Saito, Q. Guo, T. Tayagaki, K. M. Yu, and W. Walukiewicz, "Cl-doping effect in $ZnTe_{1-x}O_x$ highly mismatched alloys for intermediate band solar cells," J. Appl. Phys. **125**, 243109 (2019).
[57]J. Zhang, Y. Wang, S. Khalid, A. Janotti, G. Haugstad, and J. M. O. Zide, "Strong band gap reduction in highly mismatched alloy InAlBiAs grown by molecular beam epitaxy," J. Appl. Phys. **126**, 095704 (2019).
[58]V. Pačebutas, S. Stanionytė, R. Norkus, A. Bičiūnas, A. Urbanowicz, and A. Krotkus, "Terahertz pulse emission from GaInAsBi," J. Appl. Phys. **125**, 174507 (2019).
[59]S. Adachi, *Properties of Group-IV, III-V, and II-VI Semiconductors* (John Wiley & Sons, 2005).
[60]H. Allami, see https://github.com/hassan-allami/Lossless-HMAs for "Lossless HMAs" (2022).

Published under an exclusive license by AIP Publishing